ЖЭТФ, 2015, том 148, вып. 6 (12), стр. 1225–1231

INFRARED PHOTOLUMINESCENCE FROM GeSi NANOCRYSTALS EMBEDDED IN A GERMANIUM–SILICATE MATRIX

V. A. Volodin [a,b*], ***M. P. Gambaryan*** [a,c], ***A. G. Cherkov*** [a,b], ***V. I. Vdovin*** [a,b], ***M. Stoffel*** [d], ***H. Rinnert*** [d], ***M. Vergnat*** [d]

[a] *Rzhanov Institute of Semiconductor Physics, Siberian Branch, Russian Academy of Sciences 630090, Novosibirsk, Russia*

[b] *Novosibirsk State University 630090, Novosibirsk, Russia*

[c] *Novosibirsk State Technical University 630073, Novosibirsk, Russia*

[d] *Université de Lorraine, Institut Jean Lamour UMR CNRS 7198, B.P. 70239 54506, Vandœuvre-lès-Nancy Cedex, France*

Received April 24, 2015

We investigate the structural and optical properties of GeO/SiO_2 multilayers obtained by evaporation of GeO_2 and SiO_2 powders under ultrahigh vacuum conditions on Si(001) substrates. Both Raman and infrared absorption spectroscopy measurements indicate the formation of GeSi nanocrystals after post-growth annealing at 800 °C. High-resolution transmission electron microscopy characterizations show that the average size of the nanocrystals is about 5 nm. For samples containing GeSi nanocrystals, photoluminescence is observed at 14 K in the spectral range 1500–1600 nm. The temperature dependence of the photoluminescence is studied.

DOI: 10.7868/S0044451015120160

1. INTRODUCTION

Semiconductor nanocrystals (NCs) embedded in dielectric matrices have gained considerable scientific interest during the last decade. The investigations were mainly driven by potential applications in novel nanoelectronic and/or optoelectronic devices. Nanocrystals are characterized by physical properties that are significantly different from those of the bulk counterpart materials. For example, Si NCs embedded in a SiO_2 matrix are known to emit light in the visible–near-infrared at room temperature [1, 2] while bulk Si is unable to emit light. The Si NC related photoluminescence (PL) is well explained by charge carrier confinement in the NCs. In most cases, the optical properties of statistical ensembles of Si NCs were studied, leading to the observation of rather broad PL spectra exhibiting a full width at half maximum of a few hundreds of meV even at low temperatures. It was shown in [3] that single Si NCs are characterized by extremely narrow emission lines at low temperatures, thus demonstrating that Si NCs can be regarded as real quantum dots. While Si NCs have been extensively studied during the last decade, much less work was devoted to Ge NCs [4–8]. This is quite surprising because Ge NCs have several advantages compared to silicon NCs. Germanium has a lower melting point and consequently lower crystallization temperature than silicon. Moreover, germanium has a larger exciton Bohr radius (5 nm for Si and 24 nm for Ge). Finally, the band alignment in Ge/GeO_2 and $Ge/GeSiO_2$ heterostructures is in favor of charge carrier injection. This important feature can increase the injection efficiency for optoelectronic devices based on the Ge/GeO_2 system. Only a few works are concerned with GeSi NCs embedded in dielectric matrices [9, 10]. The properties of $Ge_xSi_{(1-x)}$ NCs are known to depend on the stoichiometry parameter x and on the NC size. Different techniques have been used to elaborate $Ge_xSi_{(1-x)}$ NCs including either

*E-mail: volodin@isp.nsc.ru

Ge and Si implantation in SiO_2 films and subsequent annealing [11] or co-evaporation of Ge, Si, and SiO_2 by radio-frequency sputtering [9].

2. EXPERIMENTAL

In this paper, we investigate the structural and optical properties of GeO/SiO_2 multilayers obtained by alternating evaporations of GeO_2 and SiO_2 powders in high vacuum (10^{-8} Torr) onto Si(001) substrates heated to 100 °C. The deposition rate of 0.1 nm/s was controlled by a quartz microbalance. The sample containing 10 periods of GeO(4 nm)/SiO_2(4 nm) was covered by a 100 nm thick SiO_2 cap layer. The sample was annealed at 800 °C in a quartz tube in high vacuum (the heating rate was 10°C·min^{-1}) during 30 minutes, after which the oven was removed and the films cooled down naturally. The stoichiometry of the layers was determined using infrared absorption spectroscopy. A Fourier transform infrared (FTIR) spectrometer FT-801 with the spectral resolution of 2 cm^{-1} was used. Raman spectra were recorded in the back-scattering geometry and the 514.5 nm Ar^+ laser line was used as the excitation source. The optical properties of the as-deposited and annealed samples were investigated by photoluminescence spectroscopy. A laser diode emitting at 488 nm was used to excite the luminescence. The PL spectra were measured using a monochromator with a grating of 600 lines/mm and a liquid nitrogen cooled InGaAs detector. All PL spectra were corrected from the response of the detector. The temperature dependence of PL was studied using a cryostat, the stability of the temperature was ±0.5 K. The procedures used for the growth and for measuring the PL are described in more detail elsewhere [10, 12]. The structural properties of the samples were investigated by transmission electron microscopy (JEM-2200FS, 200 kV accelerating voltage) using the high-resolution electron microscopy (HRTEM) and the energy dispersive spectroscopy (EDS) modes. Cross-sectional specimens were conventionally prepared by mechanical polishing with the use of Leica EM TXP, followed by ion milling.

3. RESULTS AND DISCUSSION

Figure 1 shows the IR absorption spectra of both as-deposited and annealed samples. We note that the Si substrate was used as a reference when measuring IR transmission spectra. The spectra are dominated by a main line at about 1070–1080 cm^{-1}, which may be as-

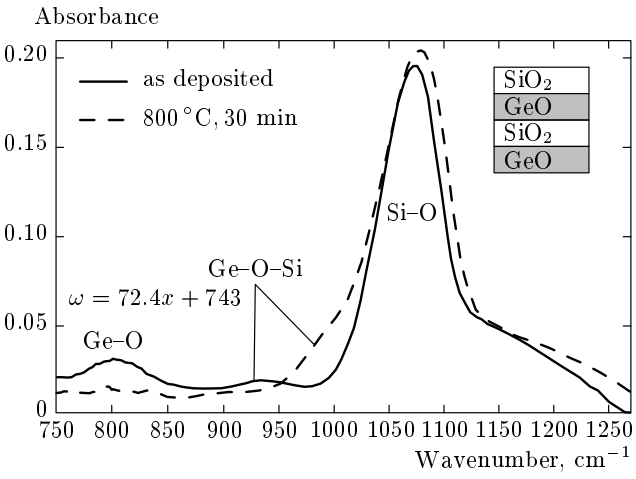

Fig. 1. IR absorption spectra of as-deposited and annealed GeO/SiO_2 multilayers. Inset: View of the as-deposited multilayer structure

cribed to the Si–O–Si stretching mode in the SiO_2 layers [13]. Another peak is observed at 805 cm^{-1} for the as-deposited sample. It may be due to the Ge–O–Ge stretching vibration mode [4, 14]. In the case of GeO_x films, this peak is known to shift approximately linearly with the stoichiometry parameter x [4, 15]. A relation between the vibration frequency ω and the stoichiometry parameter x was established in [15] in the form

$$\omega\ (\mathrm{cm}^{-1}) = 72.4x + 743.$$

In our case, the experimental peak position for the as-deposited sample is about 810 cm^{-1}. We can therefore conclude that the GeO_x films deposited at 100 °C have a stoichiometry close to that of germanium monoxide. Finally, a weak peak is observed at 940 cm^{-1}. It may correspond to Ge–O–Si vibrations. After annealing at 800 °C for 30 min, the Ge–O–Ge-related peak vanishes and the Ge–O–Si-related peak shifts to higher wavenumbers. This observation indicates that both SiO_2 and GeO layers have intermixed, leading to the formation of germanium silicate $Ge_ySi_{(1-y)}O_2$.

The cross-sectional HRTEM image of the annealed sample is shown in Fig. 2. We can clearly recognize the formation of a layer of NCs surrounded by an amorphous matrix. The average NCs size is about 5 nm. The NCs are also observed in the upper part of the structure, but their distribution is not ordered. We then perform a chemical mapping for Ge using EDS. The inset in Fig. 2 shows the occurrence of two bright bands indicating two different locations for Ge atoms.

The first band at the right corresponds exactly to the layer containing the NCs. The second band at the left may be due to Ge accumulation at the Si/SiO_2 interface. A similar observation was already made in Ge^+ implanted $Si/SiO_2/Si$ heterostructures [16].

Figure 3 shows the Raman spectra of both as-deposited and annealed samples. Since our samples are semitransparent, the Raman signal originating from the Si substrate can be observed in the studied spectral region. It is known that there are peculiarities in the range 300–420 cm^{-1} of Raman spectra that are due to two-acoustic-phonon scattering in Si substrate [17]. To suppress the background from the Si substrate, its Raman spectrum was subtracted from the Raman spectra of the samples. The Raman spectrum of the as-deposited sample does not show any peak originating from Ge–Ge bond vibrations. Therefore, the as-deposited sample does not contain Ge clusters. After annealing at 800 °C, we can see sharp peaks at 300 cm^{-1} originating from Ge–Ge vibrations and at 417 cm^{-1} due to Ge–Si vibrations. By comparing the relative intensities of these peaks [10, 18] using the formula $I_{GeGe}/I_{GeSi} = Bx/2(1-x)$, we can estimate the average composition of Ge and Si in the NCs. It was observed in [18] that the parameter B (the ratio of Raman cross-sections for Ge–Ge and Ge–Si bonds) depends on stoichiometry. In our case, $B = 1.8$ and from the experimental spectrum, we have $I_{GeGe}/I_{GeSi} = 1.5$, and hence we can conclude that NCs have the average composition $Ge_{0.6}Si_{0.4}$. For nonstressed (totally relaxed) $Ge_{0.6}Si_{0.4}$ solid alloys, the position of the Ge–Ge peak should be 290 cm^{-1} [18]. It is known that due to anharmonicity, the stiffness of distorted bonds is altered and the phonon frequencies change their values. To calculate the dependence of phonon frequencies on the strain tensor, the knowledge of anharmonicity parameters is required. This problem was solved for crystals with a diamond-type lattice [19]. With the anharmonicity parameters (in the high-symmetry cubic-lattice crystal introduced into the equations for the force matrix, there are only three such parameters, to be referred to below as p, q, and r), the phonon frequencies at the center of the Brillouin zone can be obtained from the so-called secular equation. The determinant of the resulting matrix [19, 20] should be equal to zero:

$$\begin{vmatrix} p\varepsilon_{xx}+q(\varepsilon_{yy}+\varepsilon_{zz})-\lambda & 2r\varepsilon_{xy} & 2r\varepsilon_{xz} \\ 2r\varepsilon_{xy} & p\varepsilon_{yy}+q(\varepsilon_{xx}+\varepsilon_{zz})-\lambda & 2r\varepsilon_{yz} \\ 2r\varepsilon_{xz} & 2r\varepsilon_{yz} & p\varepsilon_{zz}+q(\varepsilon_{xx}+\varepsilon_{yy})-\lambda \end{vmatrix} = 0. \quad (1)$$

Here, $\varepsilon_{\alpha\beta}$ are the components of the strain tensor, $\lambda = \Omega^2 - \omega_0^2$, Ω is the phonon frequency in the strained crystal, and ω_0 is the phonon frequency in the strain-free crystal. The difference between Ω and ω_0 ($\Delta\Omega$) being small, the phonon frequency shift $\Delta\Omega$ can be expressed as $\Delta\Omega = \lambda/2\omega_0$. In the case of a hydrostatic strained crystal ($\varepsilon_{xx} = \varepsilon_{yy} = \varepsilon_{zz} = \varepsilon_{HS}$) without twisting and shifting ($\varepsilon_{xy} = \varepsilon_{yz} = \varepsilon_{xz} = 0$), Eq. (1) can be solved:

$$2\varepsilon q + \varepsilon p - \lambda = 0. \quad (2)$$

For the frequency shift of the phonon modes with respect to the unstrained crystal, we then obtain

$$\Delta\Omega_{HS} \approx \frac{\omega_0}{2}\left(2\frac{q}{\omega_0^2} + \frac{p}{\omega_0^2}\right)\varepsilon_{HS}. \quad (3)$$

For Ge, the parameters are $p/\omega_0^2 = -1.47$, $q/\omega_0^2 = -1.93$, and $\omega_0 = 301.3$ cm^{-1} [19]. Hence, for hydrostatic stressed Ge we have $\Delta\Omega_{HS} = -803\varepsilon$. The anharmonicity parameters for Si and Ge are similar, and therefore, if we assume that these parameters are the same for GeSi solid alloys as for Ge, from the experimental shift of the Ge–Ge peak (10 cm^{-1}) we find the strain $\varepsilon_{HS} = -0.0125$, or the compressive strain 1.25 %.

The inner structure of the NCs is a problem for future investigations, and we can also assume that the Ge NCs have a Ge-rich core and a GeSi shell. Because the position of Raman peaks depends not only on the size of NCs but also on the stoichiometry [21], we cannot estimate the size, as it was done in [22].

Figure 4 shows low-temperature PL spectra of the annealed sample. The as-deposited sample does not show any PL in the IR region, and the corresponding spectrum is not shown. We can see a broad peak with a maximum at 1555 nm ($\sim$ 800 meV) and a narrow peak with a maximum at 1613 nm (769 meV). The nature of the narrow line is not clear; presumably, it can be due to $GeSi/Ge_ySi_{1-y}O_2$ interface states. This topic requires further research. The broad PL band is quite similar to the well-known PL from Ge/Si quantum well or QD structures [23, 24]. The PL intensity increases slightly when the temperature increases from 14 K to 30 K. When the temperature further increases from 30 K to 80 K, the PL intensity decreases and eventually quenching occurs at temperatures higher than 80 K.

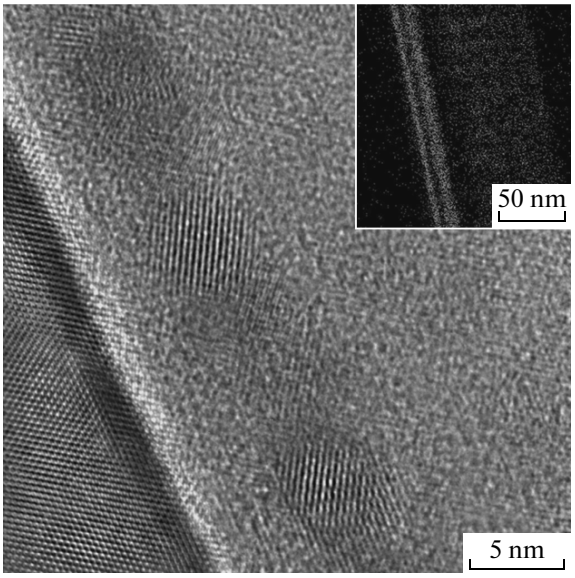

Fig. 2. HRTEM cross-sectional image of annealed GeO/SiO_2 multilayers. Inset: EDS map obtained for the Ge signal

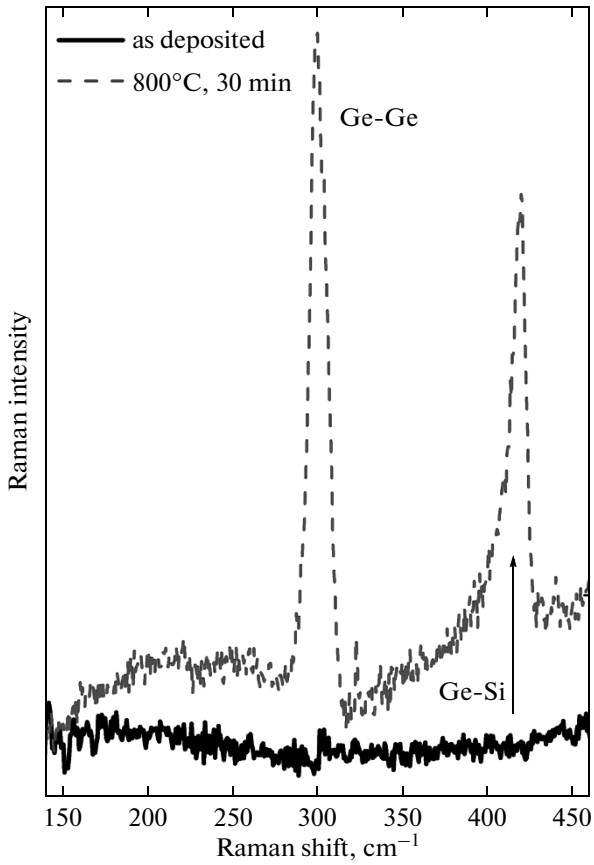

Fig. 3. Raman spectra of as-deposited and annealed GeO/SiO_2 multilayers

It is known [25] that bulk $Ge_{0.6}Si_{0.4}$ solid alloys have the energy gap 0.95 eV (1300 nm). The compressive strain leads only to enlargement of the energy gap [25], and the quantum-size effect also leads to an increase in the energy gap [6–9]. Therefore, the observed peaks (1555 and 1613 nm) can be related to defect-connected optical transitions or to optical transition in Ge–GeSi heterostructures (like core–shell), as we show in Fig. 5. If we suppose the core–shell structure, the offset of band gaps of Ge and GeSi leads to the possibility of optical transitions with the energy lower than the GeSi band gap (arrow Rad in Fig. 5). The temperature dependence of this transition can have an Arrhenius-like dependence due to the small barrier on the interface for holes localized in the Ge core. This barrier can be caused, for example, by Coulomb interaction with the charge image on the interface. As supposed above, the narrow peak at 1613 nm can be related to the optical transition between an electron in the GeSi shell and interface states on the $GeSi/GeSiO_2$ interface (arrow Rad? in Fig. 5). We note that the surrounding $GeSiO_2$ matrix is amorphous, and therefore has numerous defect states deep in the band gap and Urbach tailes in the density of states. We can suppose that there are possibilities for tunneling of electrons and holes localized in NCs and their nonradiative recombination (arrows NR in Fig. 5). It is known that the tunneling probability can depend on temperature, because the distance between tunneling-coupled centers depends on the amplitude of vibrations [26–28].

The evolution of the PL intensity as a function of temperature is shown as an inset in Fig. 4. The intensity is plotted in a logarithmic scale. Once the excitons are photogenerated, there is a competition between radiative processes and nonradiative relaxation of the photoexcited charge carriers [26, 27]. The PL intensity can be written as

$$I(T) = \frac{I_0}{1 + e_{rad}^{-1}(T) e_{nr}(T)}, \qquad (4)$$

where e_{rad} and e_{nr} are the radiative and nonradiative recombination rates, and I_0 depends on the concentration of radiative centers, the excitation photon flux, and the transition coefficient of the emitted photon from the film to air. We can assume that the dependence of the radiative recombination rate on temperature follows the Arrhenius law [26, 27], i. e., $e_{rad}(T) \propto e^{-T_a/T}$ (where T_a is the activation energy expressed in Kelvin). Since the experimentally measured PL intensity is

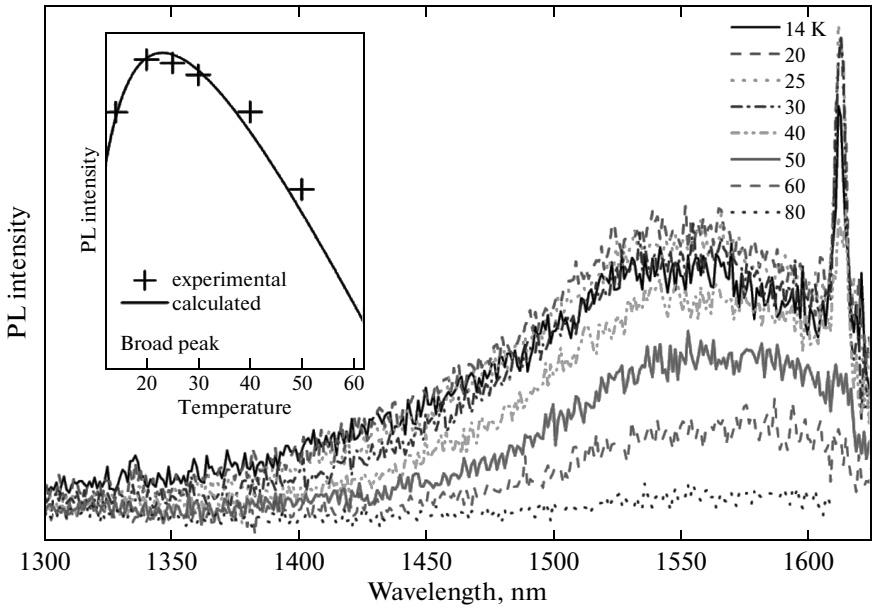

Fig. 4. Photoluminescence spectra of annealed GeO_x/SiO_2 multilayers. Inset: Experimental and calculated temperature dependencies of the PL intensity

rather low, the ratio of e_{nr} to e_{rad} is much greater than unity. Equation (4) can therefore be simplified to

$$I(T) = I_0 e_{rad}(T) e_{nr}^{-1}(T). \tag{5}$$

Finally, we can assume that the temperature dependence of the nonradiative recombination rate is defined as $e_{nr}(T) \propto e^{T/T_B}$, where T_B is the Berthelot temperature [27–32]. This equation has been successfully used to describe the evolution of the PL intensity originating from amorphous Ge quantum dots [33]. Equation (5) then becomes

$$I(T) = I_0 \exp\left\{-\frac{T}{T_B} - \frac{T_a}{T}\right\}. \tag{6}$$

All parameters I_0, T_a, and T_B were obtained by fitting the experimental data (see the inset in Fig. 4). The best fit was obtained with $T_a = 20$ K and $T_B = 26$ K. We note that there is no correspondence between the calculated and experimental data if the nonradiative recombination rate also follows an Arrhenius-like law.

The experimental and calculated data are similar to the PL temperature dependence observed for pure-Si NCs embedded in SiO_2 [28]. This fact seems to indicate that the broad PL band can be related to radiative recombinations occurring in GeSi NCs. This is further supported by the following argument. We have grown a sample consisting of 100 nm GeO followed by 100 nm of SiO_2. This structure, which was annealed in the same conditions as the GeO/SiO_2 multilayers were, is characterized by a weak Ge–Si peak in the Raman spectrum [10]. Since there is no formation of GeSi NCs in this sample, the Raman peak rather indicates that the Ge–Si alloying occurs at the Si/GeO interface and at the GeO/SiO_2 interface. We further note that no PL is observed in the spectral range 1500–1600 nm for the 100 nm GeO/100 nm SiO_2 film. We can therefore conclude that the observed PL in GeO/SiO_2 multilayers is not due to a thin Ge–Si-alloyed layer at the Si/GeO

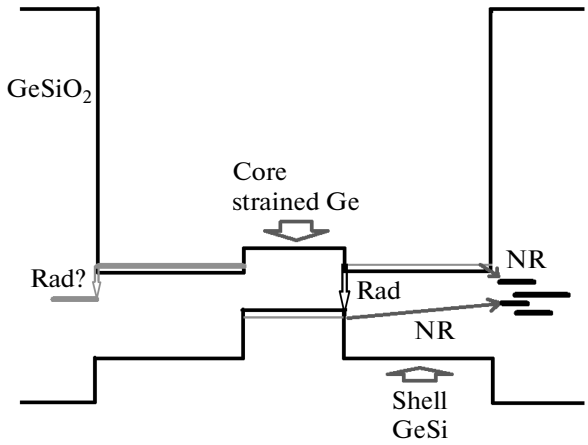

Fig. 5. Supposed scheme of radiative and nonradiative transitions

interface but can indeed be attributed to radiative recombinations of charge carriers in GeSi NCs.

4. CONCLUSIONS

We have investigated the formation of GeSi NCs in annealed GeO/SiO_2 multilayers. Post-growth annealing at 800 °C is sufficient to induce the formation of $Ge_{0.6}Si_{0.4}$ NCs having a size of about 5 nm. At low temperatures, we have observed luminescence in the spectral range 1500–1600 nm originating from radiative recombinations in GeSi NCs. PL quenching is observed for temperatures above 80 K. The temperature dependence of the PL intensity can be described well if we assume that the nonradiative recombination rate is of a Berthelot type.

This work was supported by RFBR (grant № 15-07-02298). The microscopic studies were carried out with support of Russian Federation State Contracts for provision of scientific research. V. A. V. is thankful to the administration of Université de Lorraine for a visit grant.

REFERENCES

1. T. Shimizu-Iwayama, S. Nakao, and K. Saitoh, Appl. Phys. Lett. **65**, 1814 (1994).
2. G. A. Kachurin, I. E. Tyschenko, K. S. Zhuravlev, N. A. Pazdnikov, V. A. Volodin, A. K. Gutakovsky, A. F. Leier, W. Skorupa, and R. A. Yankov, Nucl. Instr. Meth. Phys. Res. B **122**, 571 (1997).
3. I. Sychugov, R. Juhasz, J. Valenta, and J. Linnros, Phys. Rev. Lett. **94**, 087405 (2005).
4. M. Ardyanian, H. Rinnert, and M. Vergnat, J. Appl. Phys. **100**, 113106 (2006).
5. M. Ardyanian, H. Rinnert, X. Devaux, and M. Vergnat, Appl. Phys. Lett. **89**, 011902 (2006).
6. S. Takeoka, M. Fujii, S. Hayashi, and K. Yamamoto, Phys. Rev. B **58**, 7921 (1998).
7. E. G. Barbagiovanni, D. J. Lockwood, P. J. Simpson, and L. V. Goncharova, Appl. Phys. Rev. **1**, 011302 (2014).
8. E. G. Barbagiovanni, D. J. Lockwood, P. J. Simpson, and L. V. Goncharova, J. Appl. Phys. **111**, 034307 (2012).
9. S. Takeoka, K. Toshikiyo, M. Fujii, S. Hayashi, and K. Yamamoto, Phys. Rev. B **61**, 15988 (2000).
10. V. A. Volodin, D. V. Marin, H. Rinnert, and M. Vergnat, J. Phys. D: Appl. Phys. **46**, 275305 (2013).
11. K. Zhong, M. Lai, Y. Chen, and B. Gu, Physica B **407**, 3660 (2012).
12. V. A. Volodin, L. V. Sokolov, M. A. Pytyato, N. I. Petikov, M. Stoffel, H. Rinnert, and M. Vergnat, J. Appl. Phys. **115**, 053518 (2014).
13. G. Lucovsky, J. Yang, S. S. Chao, J. E. Tyler, and W. Czubatyj, Phys. Rev. B **28**, 3225 (1983).
14. G. Lucovsky, S. S. Chao, J. Yang, J. E. Tyler, R. C. Ross, and W. Czubatyj, Phys. Rev. B **31**, 2190 (1985).
15. D. A. Jishiashvili and E. R. Kutelia, Phys. Stat. Sol. (b) **143**, K147 (1987).
16. I. E. Tyschenko, M. Voelskow, A. G. Cherkov, and V. P. Popov, Semiconductors **41**, 291 (2007).
17. A. V. Kolobov, J. Appl. Phys. **87**, 2926 (2000).
18. V. A. Volodin, M. D. Efremov, A. S. Deryabin, and L. V. Sokolov, Semiconductors **40**, 1314 (2006).
19. F. Cerdeira, C. J. Buchenauer, F. H. Pollak, and M. Cardona, Phys. Rev. B **5**, 580 (1972).
20. V. A. Volodin, M. P. Sinyukov, V. A. Sachkov, M. Stoffel, H. Rinnert, and M. Vergnat, Europhys. Lett. **105**, 16003 (2014).
21. V. A. Volodin, M. D. Efremov, A. I. Yakimov, G. Yu. Mikhalev, A. I. Nikiforov, and A. V. Dvurechenskii, Semiconductors **41**, 930 (2007).
22. V. A. Volodin, D. V. Marin, V. A. Sachkov, E. B. Gorokhov, H. Rinnert, and M. Vergnat, JETP **118**, 65 (2014).
23. M. Stoffel, U. Denker, and O. G. Schmidt, Appl. Phys. Lett. **82**, 3236 (2003).
24. A. A. Shklyaev, V. I. Vdovin, V. A. Volodin, D. V. Gulyaev, A. S. Kozhukhov, M. Sakuraba, and J. Murota, Thin Solid Films **579**, 131 (2015).
25. Lianfeng Yang, Jeremy R. Watling, Richard C. W. Wilkins, Mirela Borici, John R. Barker, Asen Asenov, and Scott Roy, Semicond. Sci. Technol. **19**, 1174 (2004).
26. M. Kapoor, V. A. Singh, and G. K. Johri, Phys. Rev. B **61**, 1941 (2000).
27. D. V. Marin, V. A. Volodin, H. Rinnert, and M. Vergnat, JETP Lett. **95**, 424 (2012).

28. C. M. Hurd, J. Phys. C: Sol. St. Phys. **18**, 6487 (1985).

29. A. Yu. Kobitski, K. S. Zhuravlev, H. P. Wagner, and D. R. T. Zahn, Phys. Rev. B **63**, 115423 (2001).

30. H. Rinnert, O. Jambois, and M. Vergnat, J. Appl. Phys. **106**, 023501 (2009).

31. M. Berthelot, Ann. Chim. Phys. **66**, 110 (1862).

32. J. J. Mares, J. Kristofik, J. Pangras, and A. Hospodkova, Appl. Phys. Lett. **63**, 180 (1993).

33. A. S. Bhatti, V. N. Antonov, P. Swaminathan, J. S. Palmer, and J. H. Weaver, Appl. Phys. Lett. **90**, 011903 (2007).